Any-To-Any Connected Cavity-Mediated Architecture for Quantum Computing with Trapped Ions or Rydberg Arrays

Joshua Ramette[,1,*] Josiah Sinclair[,1] Zachary Vendeiro[,1] Alyssa Rudelis,[1] Marko Cetina,[2] and Vladan Vuletić[1]

[1] *Department of Physics, MIT-Harvard Center for Ultracold Atoms and Research Laboratory of Electronics, Massachusetts Institute of Technology, Cambridge, Massachusetts 02139, USA*

[2] *Duke Quantum Center and Department of Physics, Duke University, Durham, North Carolina 27708, USA*

We propose a hardware architecture and protocol for connecting many local quantum processors contained within an optical cavity. The scheme is compatible with trapped ions or Rydberg arrays, and realizes teleported gates between any two qubits by distributing entanglement via single-photon transfers through a cavity. Heralding enables high-fidelity entanglement even for a cavity of moderate quality. For processors composed of trapped ions in a linear chain, a single cavity with realistic parameters successfully transfers photons every few μs, increasing the interchain entanglement rate over 2 orders of magnitude beyond current methods and eliminating a major bottleneck for scaling trapped-ion systems. For one realistic scenario, we outline how to achieve the any-to-any entanglement of 20 ion chains containing a total of 500 qubits in 200 μs, with both fidelities and rates limited only by local operations and ion readout. For processors composed of Rydberg atoms, our method fully connects a large array of thousands of neutral atoms. The connectivity afforded by our architecture is extendable to tens of thousands of qubits using multiple overlapping cavities, expanding capabilities for noisy intermediate-scale quantum era algorithms and Hamiltonian simulations, as well as enabling more robust high-dimensional error-correcting schemes.

Qubit connectivity is an essential ingredient for extracting quantum advantage from a quantum computer. Whereas information propagation within a locally connected device of dimension D is limited to an effective light cone, requiring a gate depth scaling as $N^{1/D}$ for scrambling across N qubits, all-connected systems can scramble information with gate depth logarithmic in N [1–3]. Thus, nonlocal gates enable faster exploration of the device's full Hilbert space than locally connected devices, whose computational power saturates when distant qubits cannot be entangled before decoherence sets in [4]. Nonlocal gates would expand the capabilities of noisy intermediate-scale quantum (NISQ) devices to implement algorithms and simulate Hamiltonians [5] with nonlocal terms ranging from qubit-based encodings of the fermionic molecular Hamiltonian [6] to dual quantum gravity models

[7] and other systems with qualitatively different dynamical behaviors due to fast information scrambling [8–10]. Beyond the NISQ era, full connectivity is favorable for quantum error correction, increasing error thresholds [11] and enabling high-dimensional codes with favorable scalings of logical qubit encoding rates and codeword distances [12–15].

Connectivity inherently conflicts with scalability, since having both requires either a high-dimensional topology or infinite-range interactions. For example, while in Rydberg atom arrays qubit numbers have rapidly increased to over 250 [16–20], connectivity so far remains limited to a few neighboring atoms within the Rydberg blockade radius [20–22]. In contrast, linear trapped ion chains, which natively support full connectivity via the collective motion of the chain, have seen slow increases in qubit number due to gate fidelities degrading with chain size [23,24], and challenges connecting multiple ion chains together. Current experiments have demonstrated intermodule connection based on ion shuttling [25,26] and photonic interconnects [27–32] with rates far below local operation speeds (though faster rates might be reached with cavity-enhanced collection [33–35]). As a result, only very small fully connected NISQ devices have been experimentally realized [23,24,36].
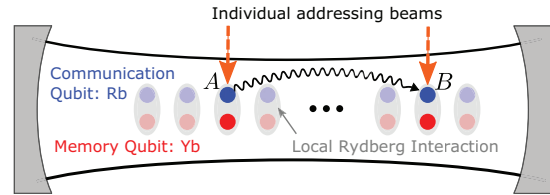
---

*jramette@mit.edu; joshuaramette@gmail.com

In this paper, we propose a new architecture for quantum computing, which takes small, high-fidelity, local quantum processors, places them inside an optical cavity, and quickly connects them using heralded single-photon transfers. We examine specific implementations of our approach with a cavity of moderate volume and quality for both trapped ions and Rydberg arrays. First, we show that with direct single-photon transfers through the cavity, we can connect ion chains with speeds hundreds of times faster than is currently possible with existing approaches, eliminating a major bottleneck currently limiting trapped-ion system sizes (see Fig. 4). We outline one specific proposal for a fully connected trapped-ion system containing 20 chains and 500 ions with both gate fidelity and speed limited by local Coulomb operations and state readout, rather than the ion-cavity coupling. For Rydberg arrays, we show that our scheme can be used to provide arbitrary connectivity for up to 1500 neutral-atom qubits along with fast cavity-mediated, nondestructive readout. Our architecture is extendable to multiple overlapping cavities containing tens of thousands of trapped ions or Rydberg qubits. It also enables state readout for individual qubits within a few tens of microseconds.

Previous proposals to engineer gates via optical cavities have been susceptible to photon losses, and have consequently required stringent experimental parameters in terms of cavity finesse and/or high-fidelity single-photon sources. Schemes enacting nonlocal gates through direct transfers of photons between atoms [37] have errors, which scale poorly with the cooperativity (C) as $1/\sqrt{C}$ [38], or success probabilities with similar scaling for heralded schemes [39]. Alternative schemes where the phase of a reflected photon flips depending on the internal state of atoms coupled to a cavity mode [40–42] require high-fidelity single-photon sources. In contrast, our scheme employs gate teleportation to avoid a direct coupling of the quantum register to the common cavity mode, protecting the quantum information from the decoherence associated with optical losses. Gate teleportation has previously been proposed to connect ion chains in separate modules [43,44], but relied on slow, two-photon entanglement generation.

In Figs. 1(a) and 1(b), we consider a set of local processors composed of communication qubits and memory qubits. Communication qubits are coupled to the cavity and used for distribution of entanglement, while memory qubits couple to communication qubits via a local interaction [Rydberg interaction shown in (a) and Coulomb interaction shown in (b)]. Photon-loss processes associated with the cavity linewidth κ and atomic state scattering associated with the atomic linewidth Γ compete with the atom-cavity coupling g to determine the success probability for entangling communication qubits. Each local processor is referred to as a node, such that in the figure, nodes A and B represent any two local processors within

(a) Any-to-Any-Connected Rydberg Processors

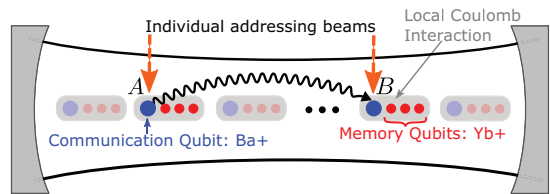**(b)** Any-to-Any-Connected Ion Processors

FIG. 1. Architecture for cavity-mediated quantum gate between any two qubits applied to (a) Rydberg atoms or (b) multiple chains of trapped ions. Photon transfers via the cavity produce heralded entanglement of communication qubits. Local interactions between communication and memory qubits enable teleported gates between any two memory qubits. Different atomic species can be used for the communication and memory qubits so that the latter remain unaffected during the entanglement process for communication qubits.

the cavity mode volume. Executing a teleported CNOT gate [45,46] between any two qubits within our architecture requires the following steps, shown in Fig. 2:

(1) Create a Bell state between the communication qubits at nodes A and B by (i) and (ii) passing a photon from A to B via a (lossy) cavity. With a carefully designed transfer protocol, measuring an empty ground state of B ensures, without destroying the established entanglement, that the photon has not been lost due to cavity or atomic excited-state decays. This leaves the communication qubits at A and B projected into a Bell state (iii).

(2) Once the nonlocal Bell pair is established, enact local CNOT gates between communication and memory qubits at nodes A and B, then measure the states of the A and B communication qubits. Based on the results, enact single-qubit gates to realize a teleported CNOT gate between memory qubits at nodes A and B.

I. ENTANGLEMENT DISTRIBUTION SCHEME

We now describe a protocol to establish a Bell pair between any two communication qubits at nodes A and B with, in principle, unit fidelity despite cavity (κ) and atomic scattering (Γ) loss mechanisms. The level structure we assume for communication and memory qubit atoms is shown in Fig. 3. We assume that while $|e\rangle$ has

Any-to-Any-Connected Teleported CNOT Gate

(1) Distribute Entanglement

(i) Photon released from A.

(ii) B absorbs photon unless it escapes from the cavity.

(iii) Measuring empty B ground state heralds successful transfer and entanglement.

(2) Following successful entanglement of A+B, local Rydberg and ion gates enable gate teleportation.
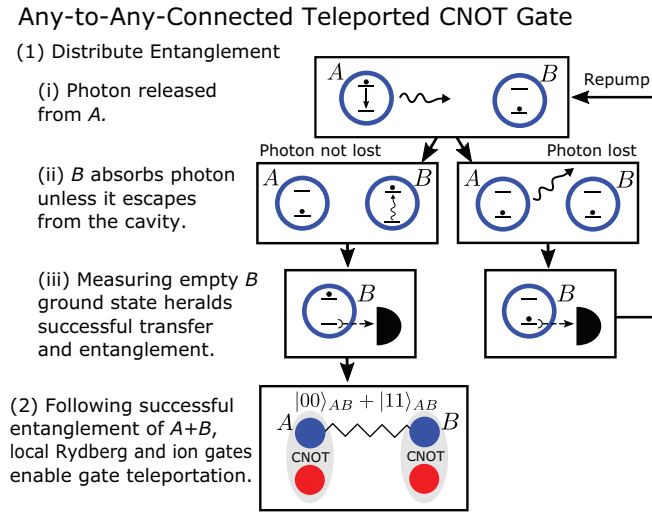
FIG. 2. Heralded photon transfers create entanglement between distant communication qubits. Subsequent high-fidelity local operations enable teleported quantum gates between distant memory qubits.

a linewidth Γ, scattering back into $|r_0\rangle$ or $|r_1\rangle$ (which we call "operation states" and could be Rydberg states in a realization with neutral atoms) is strongly suppressed, so that all scattering- and photon-loss events are detectable by leaving B in the ground states $|0\rangle$ or $|1\rangle$.

Our protocol to generate the Bell pair begins in the state

$$|\Psi\rangle = \frac{1}{\sqrt{2}}(|r_0\rangle_A + |r_1\rangle_A)|0\rangle_B|\text{vac}\rangle_E, \tag{1}$$
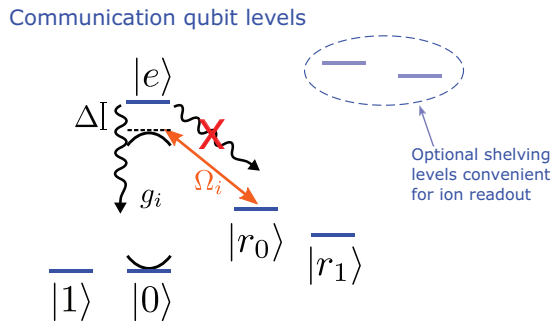
Communication qubit levels

FIG. 3. Atomic level scheme for the communication qubits. The communication qubits are coupled to the cavity with strength g_i and addressed individually with Rabi frequency Ω_i. The excited state $|e\rangle$ decays at Γ, and the level and addressing schemes are chosen to suppress the probability of decay into the operation states $|r_0\rangle$ and $|r_1\rangle$. Raman transitions or microwaves enable site selective rotations between the qubit states $|0\rangle$ and $|1\rangle$ and between the operation states $|r_0\rangle$ and $|r_1\rangle$. For trapped ions, long-lived shelving levels can be used as part of the heralding process. For Rydberg atoms, Rydberg levels conveniently act as operation states.

where all other communication qubits are stored in state $|1\rangle$ so they do not couple to the cavity, and the environment E of modes external to the cavity is in the vacuum state. Then, a photon is transferred through the cavity from A to B, conditioned on A being in $|r_0\rangle_A$. The transfer is done either using two-photon Raman π pulses with nonzero detuning Δ to release a photon from A and absorb it at B, or with resonant stimulated Raman adiabatic passage (STIRAP) [47] by ramping up Ω_A while ramping down Ω_B [37]. During this transfer, the photon may leak out of the cavity, or may scatter off of $|e\rangle_A$ or $|e\rangle_B$. Therefore, we have $|r_0\rangle_A|0\rangle_B|\text{vac}\rangle_E \rightarrow \alpha|0\rangle_A|r_0\rangle_B|\text{vac}\rangle_E + \beta|\text{Loss}\rangle$, where $|\text{Loss}\rangle$ represents a generic state of the form $\sum_{k,l,\mu} \alpha_{kl\mu}|k\rangle_A|l\rangle_B \hat{a}_\mu^\dagger|\text{vac}\rangle_E$ where the photon has scattered into a mode μ outside the cavity and the atoms A and B are left in some collection of ground states indexed by k and l. Since the ground states are only coupled via the cavity mode for the remainder of the protocol, once in the state $|\text{Loss}\rangle$, atoms A and B cannot evolve out of their ground states. Thus a state $|\text{Loss}\rangle$ maps to $|\text{Loss}\rangle$ under further operations in the protocol. The lossy transfer results in the following state:

$$|\Psi\rangle = \frac{1}{\sqrt{2}}(\alpha|0\rangle_A|r_0\rangle_B|\text{vac}\rangle_E + \beta|\text{Loss}\rangle)$$
$$+ \frac{1}{\sqrt{2}}|r_1\rangle_A|0\rangle_B|\text{vac}\rangle_E. \tag{2}$$

We repeat the transfer on the other component in the Bell state to symmetrize the losses. First swap the two states $|r_0\rangle$ and $|r_1\rangle$ on A and B and also swap the two ground states on A:

$$|\Psi\rangle = \frac{1}{\sqrt{2}}(\alpha|1\rangle_A|r_1\rangle_B|\text{vac}\rangle_E + \beta|\text{Loss}\rangle)$$
$$+ \frac{1}{\sqrt{2}}|r_0\rangle_A|0\rangle_B|\text{vac}\rangle_E. \tag{3}$$

Then, execute a second identical STIRAP as before, which affects only the last term in Eq. (3). Assuming the loss is symmetrized by using the same temporal profiles for Ω_A and Ω_B as before, this results in the same values for α and β (where $|\text{Loss}'\rangle$ denotes the state where the photon is scattered during the second STIRAP):

$$|\Psi\rangle = \frac{1}{\sqrt{2}}(\alpha|1\rangle_A|r_1\rangle_B|\text{vac}\rangle_E + \beta|\text{Loss}\rangle)$$
$$+ \frac{1}{\sqrt{2}}(\alpha|0\rangle_A|r_0\rangle_B|\text{vac}\rangle_E + \beta|\text{Loss}'\rangle),$$
$$= \alpha\frac{1}{\sqrt{2}}(|1\rangle_A|r_1\rangle_B + |0\rangle_A|r_0\rangle_B)|\text{vac}\rangle_E$$
$$+ \beta\frac{1}{\sqrt{2}}(|\text{Loss}\rangle + |\text{Loss}'\rangle). \tag{4}$$

Within the α component of $|\Psi\rangle$, A and B are now entangled. As shown in Fig. 2, measuring whether or not atom B occupies a ground state projects $|\Psi\rangle$ either into $|\text{Loss}\rangle$ or into the Bell state $(|1\rangle_A |r_1\rangle_B + |0\rangle_A |r_0\rangle_B)/\sqrt{2}$.

II. EXPERIMENTAL IMPLEMENTATIONS

We demonstrate the feasibility of our approach by outlining specific implementations using commonly trapped species of ions and Rydberg atoms. We simulate the transfer dynamics by coupling two atoms or ions to the cavity mode and addressing them via a STIRAP pulse sequence of duration T with Gaussian pulses of peak strength Ω_0. The success probability forms a landscape over the space of Ω_0 and T values, where each point in the space represents a trade-off between excited-state losses (Γ) and cavity losses (κ). With cavities comparable to those used in existing experiments, we show how to realize few-μs transfer times with reasonable success probability (40%) even with cavity mode volumes large enough to trap many atoms and ions. We also describe the leading expected error sources of the nonlocal gates and how our scheme's symmetry improves the fidelity of the Bell state.

The scheme is designed to be robust against slow variations in the laser and cavity coupling strengths (which may slightly affect the success probability but not the heralded fidelity), and does not require identical coupling strengths at any of the nodes. This allows entanglement even between communication qubits trapped over a broad range of positions within a spatially varying cavity-mode profile.

Broadly, the errors of the two local gates (ϵ_{local}) as well as those of the two communication qubit readout measurements (ϵ_M) and the infidelity of the distributed Bell state (ϵ_{Bell}) all contribute to the overall nonlocal gate error: $\epsilon_{\text{CNOT}} = 2\epsilon_{\text{local}} + 2\epsilon_M + \epsilon_{\text{Bell}}$. However, our scheme's two repeated transfers through the same cavity mode symmetrize the amplitudes on the two components of the heralded Bell pair despite photon losses. This makes the process insensitive to asymmetries and slow drifts in the coupling strengths and requires repeatability of the couplings only on the few-μs timescale. While laser-pulse strength and phase fluctuations could introduce imperfections, excellent phase coherence over the few microseconds of optical control used in our scheme is possible, as evidenced by the long optical qubit coherence times routinely demonstrated [48]. Our scheme can also be made first-order insensitive to laser amplitude fluctuations by choosing the optimal value for Ω_0 within the success probability landscape (see the Supplemental Material [49]).

A. Application to trapped ions

An implementation for local trapped-ion processors could use Ba$^+$ ions as communication qubits and Yb$^+$ ions as memory qubits (these two species are favorable for

implementing interspecies local operations [31], although many other species combinations are possible, such as using different Ba$^+$ isotopes for communication and memory). This does not introduce extra complexity, as a second ion species is likely already necessary for sympathetic cooling in any trapped-ion system and can also function as our communication qubits [31]. To realize the level scheme depicted in Fig. 3, we use the ^{137}Ba$^+$ isotope with nuclear spin $I = 3/2$. The operation states $|0\rangle$ and $|1\rangle$ in Fig. 3 correspond to the clock states $|F = 2, m_F = 0\rangle$ and $|F = 1, m_F = 0\rangle$ in the $6S_{1/2}$ ground-state manifold, and the states $|r_0\rangle$ and $|r_1\rangle$ correspond to $|F = 2, m_F = 0\rangle$ and $|F = 0, m_F = 0\rangle$ in the metastable $5D_{3/2}$ state manifold, while the excited state $|e\rangle$ is the state $|F = 3, m_F = 0\rangle$ in $6P_{3/2}$. Then rotations between $|0\rangle$ and $|1\rangle$ and between $|r_0\rangle$ and $|r_1\rangle$ can be driven via Raman transitions [50]. The states $|r_0\rangle$ and $|r_1\rangle$ in $5D_{3/2}$ are chosen because
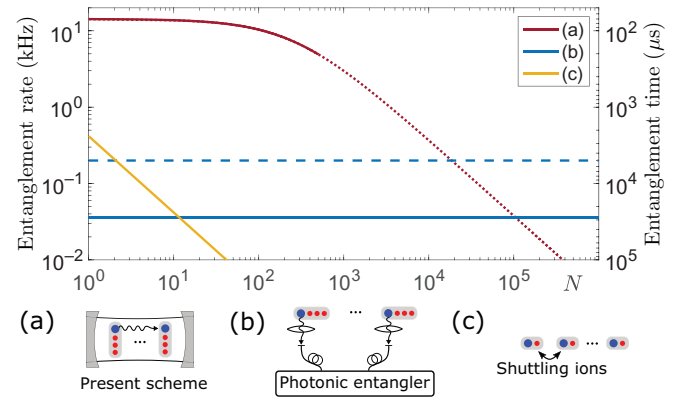

FIG. 4. Comparison of the average rates for distributing entanglement to M any-to-any-connected local processors comprising N total qubits for different modalities (a)–(c). (a) Red line: intracavity entanglement method proposed here with 25 ions per chain using the parameters outlined in this section, with the entanglement time given by $(\tau_{\text{parallel}} + \frac{1}{2}M\tau_{\text{serial}})/p$, and where $p = 0.40$, $\tau_{\text{serial}} = 5.3$ μs (see the Supplemental Material [49]), and $\tau_{\text{parallel}} = 28$ μs [52]. The red line changes from solid to dashed at $N = 500$, representing the number of ions that could be fit comfortably in a single rf trap along the cavity axis. (b) Blue lines: photonic interconnects with 25 ions per chain using the method of Refs. [29,31,53] can entangle many pairs of ion chains in parallel if the photons are routed through an optical cross-connect switch. The dashed blue line shows the current state of the art for entangling two ions (5 ms) [32], and the solid blue line shows the same with additional realistic overheads necessary for achieving high-fidelity full connectivity, including a factor of 2 overhead for entanglement purification [32,54], cross-connect switch insertion losses (1.3 dB per photon), and switching time (10 ms overhead) [55,56]. (c) Yellow line: ion shuttling architectures [57,58], where ions are physically transported between different ion traps, require milliseconds of sympathetic re-cooling after each split/merge operation. Demonstrated geometries (two ions per local processor, see [25]) lead to linearly increasing transport time for fully connected circuits.

of the small branching ratio from $6P_{3/2}$ to $5D_{3/2}$ [51], which strongly suppresses spontaneous decay back into $|r_0\rangle$ and $|r_1\rangle$.

The cavity is tuned on resonance with the $|0\rangle \rightarrow |e\rangle$ transition at 455 nm, at which wavelength we would expect losses in the mirrors of 2×10^{-5} to be achievable [59]. With these mirror losses, a cavity of length $L = 2.8$ mm with a 13-μm Gaussian-mode waist would have a Rayleigh range of 1170 μm, a linewidth $\kappa = 2\pi \times 340$ kHz, and finesse $\mathcal{F} = \pi c/(L\kappa) = 157\,000$, and would give a coupling strength between the ion and the cavity at the center of the mode of $g = 2\pi \times 5.8$ MHz. With an excited state linewidth of $\Gamma = 2\pi \times 25$ MHz, this gives a cavity cooperativity $C = g^2/\kappa\Gamma = 3.9$. While success probability asymptotically scales like $1/\sqrt{C}$ for large cooperativity [38], with a cooperativity on the order of unity, the coupling strength g to the cavity mode is of similar strength to the geometric mean of the loss processes $\sqrt{\kappa\Gamma}$, meaning we expect on the order of half the transfer attempts to be successful (see the Supplemental Material [49] for discussion of transfer success dependence on cavity quality). A simulated photon transfer with these parameters gives an efficiency of around $p = 0.40$ over 1.0 μs, making it possible to establish entanglement between any two Ba$^+$ ions on the microsecond timescale with a laser pulse profile with a peak strength of $\Omega_0 = 2\pi \times 18$ MHz. A cavity with these parameters could be integrated with a single rf surface ion trap (with dc segmentation) oriented along the cavity axis [60], with the ions located about 70 μm above the surface, and with 200-μm space between each mirror and the closest ion [33]. For chains of 25 ions, each of length 88 μm with 3.5 μm interion spacing and 30 μm of space between chains, this configuration would fit 20 chains along the cavity axis (for a total of 500 qubits) within the Rayleigh range of the cavity mode. Each ion chain is positioned so that its single communication qubit sits directly on a cavity mode antinode, where the cavity field strength is relatively insensitive to the ion position [61].

Across all chains, the entanglement generation process would consist of a serial stage, where fast cavity transfers are carried out between all M chains, followed by a stage of parallelized fluorescence readout to verify transfer success and herald entanglement. Then, local operations in successfully heralded pairs, performed between communication and memory qubits, can directly use the entanglement for teleported gates, or can swap the entanglement onto other ions in the chain for later use. A full quantum gate circuit is implemented by repeated iterations of the above steps.

Following each fast cavity transfer in the serial stage, the logical states of both A and B can be shelved in $|5D_{5/2}, F = 1, m_F = 0\rangle$, and $|5D_{5/2}, F = 2, m_F = 0\rangle$ using Raman transitions. Shelving ensures atom A does not couple to the cavity during subsequent transfers and prevents atom B from scattering into the operation states during

standard fluorescence readout on $6P_{1/2}$. The entire attempt, including shelving, requires approximately $\tau_{\text{serial}} \approx 5$ μs per pair of communication qubits (see the Supplemental Material [49]). Readout for heralding can then be done in parallel across all the pairs in a time $\tau_{\text{parallel}} \approx 28$ μs [52]. On average, pM of the chains are entangled in time $\tau_{\text{parallel}} + M\tau_{\text{serial}}/2$, so that the average amount of time taken to distribute $M/2$ Bell pairs among the $M/2$ pairs of chains is $(\tau_{\text{parallel}} + M\tau_{\text{serial}}/2)/p$.

For small τ_{serial}, even for moderately large M the entanglement distribution and nonlocal gate speed is on the order of local Coulomb gates and readout (tens of μs [48]). Figure 4 shows how for the parameters described here, our scheme is limited primarily by the readout time τ_{parallel} for system sizes up to a few hundred qubits, and can distribute entanglement between 20 chains comprising 500 qubits in an average of 200 μs. The local gate errors are expected to dominate the overall teleported gate infidelity [see the Supplemental Material [49] for discussion of mitigating contributions from entanglement preparation such as backscattering (10^{-3}), single-qubit rotations (4×10^{-3}), and thermal motion (10^{-2})] for the parameters outlined here. With the ability to link multiple chains at speeds and fidelities comparable to local gates, large trapped-ion quantum computers will enable NISQ applications far exceeding what is currently possible.

B. Application to Rydberg arrays

As an example of a realization with realistic parameters in neutral atoms with local Rydberg gates, consider a dual-species experiment where for the communication qubits we use ^{87}Rb (which can conveniently couple to a high-finesse cavity in the near infrared), and for the memory qubits we use ^{171}Yb (where the magnetically insensitive, metastable nuclear spin states $|^3P_0, m_F = \pm 1/2\rangle$ with lifetime $\tau = 26$ s function as logical states from which the Rydberg states are accessible via a single-photon transition). For the network ^{87}Rb atoms, $|5S_{1/2}, F = 1, m_F = 0\rangle$ and $|5S_{1/2}, F = 2, m_F = 0\rangle$ are the logical $|0\rangle$ and $|1\rangle$ states, and the cavity at 780 nm couples $|5S_{1/2}, F = 2, m_F = 0\rangle$ to $|e\rangle = |5P_{3/2}, F = 3, m_F = 0\rangle$. High-lying Rydberg states of the form nS and nP with $n \geq 70$ are used for $|r_0\rangle$ and $|r_1\rangle$, which are coupled by microwave radiation. We choose a cavity with a length $L = 2$ cm (where the centimeter-scale cavity keeps the atoms far from the mirrors to mitigate any effects of stray electric fields [63]) and moderate finesse $\mathcal{F} = 140\,000$ for a ring-down time 3.0 μs and cavity linewidth $\kappa = 2\pi \times 53$ kHz. We assume a Gaussian mode with waist 10 μm and coupling strength $g = 2\pi \times 2.8$ MHz at the center of the Gaussian mode, so that with the ^{87}Rb natural linewidth of $2\pi \times 6$ MHz we have a cavity of moderate cooperativity $C = 25$ with a Rayleigh range of $z_R = 403$ μm.

Simulating the STIRAP transfer efficiency with these cavity parameters, we achieve a successful transfer probability of $p = 0.67$ in 2.5 μs with $\Omega_0 = 2\pi \times 8.6$ MHz. The total time spent to establish a Bell pair (two separate cavity-mediated transfers in the protocol) is then around $(1/0.67) \times 2 \times 2.5\ \mu\text{s} \approx 7\ \mu\text{s}$.

The Rydberg states, already necessary for the local Rydberg gates, naturally realize the scattering suppression indicated in Fig. 3. The Rydberg states with typical lifetimes of a few hundred μs would occasionally decay during the few-μs transfer, but these small losses again can be symmetrized away and heralded with our scheme. This ensures that no distortion of the heralded Bell state occurs, as both components of the Bell state can be made to spend the same amount of time in the Rydberg states. Entanglement distribution failures are measured at atom B following the transfer attempt by quickly depumping $F = 1$, then moving $|r_0\rangle_B$ and $|r_1\rangle_B$ into the $F = 1$ manifold and using a broadband laser and a single microwave frequency to couple the broad set of Rydberg states thermally accessible from $|r_0\rangle_B$ and $|r_1\rangle_B$ to the $F = 3$ excited state, from where it would decay to the $F = 2$ ground state. Transfer failure due to cavity losses or Rydberg decays then results in an $F = 2$ ground state atom B.

Nondestructive fluorescence imaging of dipole-trapped neutral atoms typically takes milliseconds [64], much slower than for ions. However, the cavity itself can enable fast serial state readout [65–68]. For example, probing the cavity transmission on the nearly closed $|5S_{1/2}, F = 2\rangle$ to the $|5P_{3/2}, F = 3\rangle$ transition can be much faster, with readout speed limited only by the cavity ringdown time (here 3 μs) and the necessity to avoid saturation [65] (which would occur only here with an incident probe photon rate beyond $g^2/\kappa \approx 10^3\ \mu\text{s}^{-1}$).

With a 2.6-μm spacing between sites [69] and assuming probabilistic loading of both species with no rearrangements and 50% atom filling, such that the probability of loading both a ^{87}Rb and a ^{171}Yb is 25%, this allows approximately 75 qubits in a one-dimensional (1D) chain along the cavity-mode axis within $\pm z_R$. (With rearrangement of both species this number would be 300 qubits.) One more row of qubits to each side of the axis could easily fit in a rectangular lattice within the 6 μm before the mode function falls off by $1/\sqrt{2}$ radially for a total of approximately 225/900 qubits without and with rearrangement. With rows in a triangular pattern [70] with 2.6-μm lattice spacing, we could fit five total rows of atoms with no atoms more than 4.5 μm radially distant from the mode axis, for a total of approximately 325/1500 qubits without and with rearrangement.

In Fig. 5(a) we compare a Rydberg array limited to nearest-neighbor gates to our cavity-mediated architecture that represents a serial, any-to-any connected system. The average nonlocal gate fidelity in the nearest-neighbor architecture degrades with increasing system size due
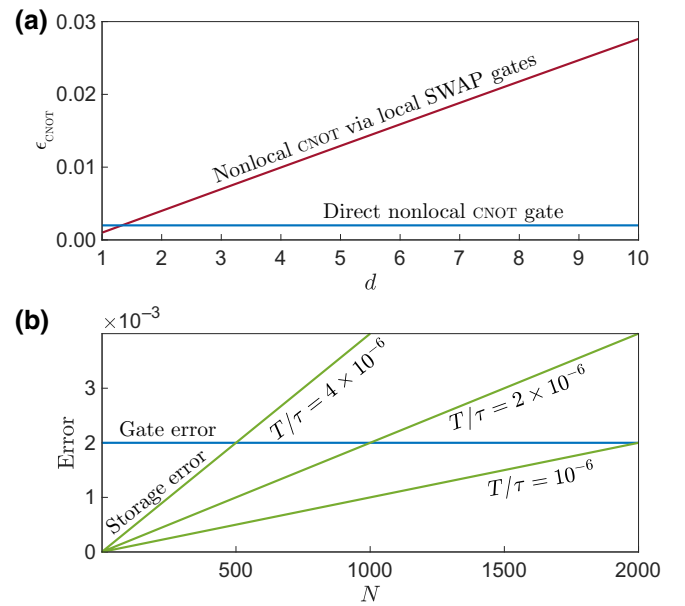

FIG. 5. With nearest-neighbor Rydberg gate errors of $\epsilon_R = 10^{-3}$ [62], the nonlocal teleported CNOT gate error is limited to $\epsilon_{\text{CNOT}} \sim 2\epsilon_R = 2 \times 10^{-3}$ (a) Error probabilities due to local two-qubit gate errors for gates between qubits d sites apart, when implemented directly via teleportation (constant error ϵ_{CNOT}, solid blue) or via local SWAP gates [red, three local CNOT gates per SWAP gate for an error $\epsilon_R + 3(d-1)\epsilon_R$]. (b) Comparing storage and gate errors for implementing serial any-to-any gates. The serial system can be scaled until $NT/\tau \sim \epsilon_{\text{CNOT}}$ before storage errors would dominate gate errors.

to the increasing number of local SWAP gate errors. In Fig. 5(b), we consider the effect of the nonlocal gate speed on qubit storage errors in a serial, any-to-any connected system. During each two-qubit gate of duration T with qubits of lifetime τ, there is probability NT/τ of a qubit storage error among the N qubits.

Note that in locally connected systems, the SWAP gate overheads can lead not only to more local gate errors, but also more storage errors due to the extra time required to sequentially implement the SWAP gates. In general, the time required to perform N nonlocal gates across the N qubits depends on both the degree of connectivity and parallelizability. Local systems in finite dimensions require increasing amounts of parallelization to equal or exceed the runtime and storage error performance of serial any-to-any connected systems (see the Supplemental Material [49] for a more quantitative comparison).

III. CONCLUSIONS AND OUTLOOK

We have presented a new architecture for connecting many local quantum processors within a single optical cavity, and outlined feasible implementations of our scheme with local processors composed of linear chains of trapped ions or neutral Rydberg atoms. For both Rydberg atoms and trapped ions, our scheme makes it possible to create
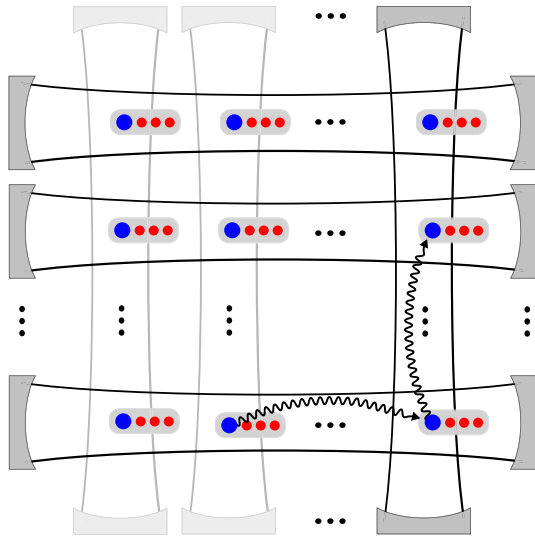
FIG. 6. Extension to larger systems. The methods outlined here could be extended using several overlapping cavity modes, creating systems with potentially 10^4 all-connected qubits. Several vertical cavity modes (shaded) provide parallelization, such that many photon transfers can be accomplished simultaneously. Any two communication ions can be entangled in two steps, by photon-mediated communication along a horizontal and a vertical cavity mode.

all-connected quantum systems of several hundred qubits within a single optical cavity with realistic parameters.

Our methods can easily be extended to multiple overlapping cavity modes with modest overheads in entanglement distribution speeds, allowing thousands of fully connected trapped ion or Rydberg qubits (see Fig. 6). With hundreds to thousands of fully connected qubits, many more NISQ simulations become feasible. Beyond the NISQ era, any-to-any connectivity in systems with many qubits may allow the realization of logical qubits using some of the most promising quantum codes, and we hope that our proposal inspires additional theoretical investigation into optimal codes unlimited by connectivity constraints. Once localized modules containing logical qubits are constructed, slower entanglement methods like two-photon entanglement distribution [29,31,71] can then be used to connect those longer-lived logical-qubit modules into even larger systems.

Note added.—We have recently become aware of an alternative effort to endow Rydberg arrays with any-to-any connectivity using atom shuttling [72].

[1] Y. Sekino and L. Susskind, Fast scramblers, J. High Energy Phys. **2008**, 065 (2008).

[2] W. Brown and O. Fawzi, Scrambling speed of random quantum circuits (2013), ArXiv:1210.6644.

[3] S. Boixo, S. V. Isakov, V. N. Smelyanskiy, R. Babbush, N. Ding, Z. Jiang, M. J. Bremner, J. M. Martinis, and H. Neven, Characterizing quantum supremacy in near-term devices, Nat. Phys. **14**, 595 (2018).

[4] Y. Zhou, E. M. Stoudenmire, and X. Waintal, What Limits the Simulation of Quantum Computers?, Phys. Rev. X **10**, 041038 (2020).

[5] E. Altman, *et al.*, Quantum simulators: Architectures and opportunities, PRX Quantum **2**, 017003 (2021).

[6] B. Bauer, S. Bravyi, M. Motta, and G. K.-L. Chan, *Report on the NSF Workshop on Enabling Quantum Leap: Quantum algorithms for quantum chemistry and materials*, Tech. Rep. (2019).

[7] L. García-Álvarez, I. L. Egusquiza, L. Lamata, A. del Campo, J. Sonner, and E. Solano, Digital Quantum Simulation of Minimal AdS/CFT, Phys. Rev. Lett. **119**, 040501 (2017).

[8] S. Bravyi, M. B. Hastings, and F. Verstraete, Lieb-Robinson Bounds and the Generation of Correlations and Topological Quantum Order, Phys. Rev. Lett. **97**, 050401 (2006).

[9] M. Foss-Feig, Z.-X. Gong, C. W. Clark, and A. V. Gorshkov, Nearly Linear Light Cones in Long-Range Interacting Quantum Systems, Phys. Rev. Lett. **114**, 157201 (2015).

[10] G. Bentsen, T. Hashizume, A. S. Buyskikh, E. J. Davis, A. J. Daley, S. S. Gubser, and M. Schleier-Smith, Treelike Interactions and Fast Scrambling with Cold Atoms, Phys. Rev. Lett. **123**, 130601 (2019).

[11] K. M. Svore, B. M. Terhal, and D. P. DiVincenzo, Local fault-tolerant quantum computation, Phys. Rev. A **72**, 022317 (2005).

[12] N. Baspin and A. Krishna, Connectivity constrains quantum codes (2021), ArXiv:2106.00765.

[13] N. P. Breuckmann and V. Londe, Single-shot decoding of linear rate ldpc quantum codes with high performance (2020), ArXiv:2001.03568.

[14] S. Bravyi and R. König, Classification of Topologically Protected Gates for Local Stabilizer Codes, Phys. Rev. Lett. **110**, 170503 (2013).

[15] S. Bravyi and B. Terhal, A no-go theorem for a two-dimensional self-correcting quantum memory based on stabilizer codes, New J. Phys. **11**, 043029 (2009).

[16] L. Henriet, L. Beguin, A. Signoles, T. Lahaye, A. Browaeys, G.-O. Reymond, and C. Jurczak, Quantum computing with neutral atoms, Quantum **4**, 327 (2020).

[17] K.-N. Schymik, V. Lienhard, D. Barredo, P. Scholl, H. Williams, A. Browaeys, and T. Lahaye, Enhanced atom-by-atom assembly of arbitrary tweezer arrays, Phys. Rev. A **102**, 063107 (2020).

[18] P. Scholl, M. Schuler, H. J. Williams, A. A. Eberharter, D. Barredo, K.-N. Schymik, V. Lienhard, L.-P. Henry, T. C. Lang, T. Lahaye, A. M. Läuchli, and A. Browaeys, Quantum simulation of 2d antiferromagnets with hundreds of Rydberg atoms, Nature **595**, 233 (2021).

[19] G. Semeghini, H. Levine, A. Keesling, S. Ebadi, T. T. Wang, D. Bluvstein, R. Verresen, H. Pichler, M. Kalinowski, R. Samajdar, A. Omran, S. Sachdev, A. Vishwanath, M. Greiner, V. Vuletic, and M. D. Lukin, Probing topological spin liquids on a programmable quantum simulator (2021), ArXiv:2104.04119.

[20] D. Bluvstein, A. Omran, H. Levine, A. Keesling, G. Semeghini, S. Ebadi, T. T. Wang, A. A. Michailidis, N. Maskara, W. W. Ho, S. Choi, M. Serbyn, M. Greiner, V. Vuletić, and M. D. Lukin, Controlling quantum many-body dynamics in driven Rydberg atom arrays, Science **371**, 1355 (2021).

[21] H. Bernien, S. Schwartz, A. Keesling, H. Levine, A. Omran, H. Pichler, S. Choi, A. S. Zibrov, M. Endres, M. Greiner, V. Vuletić, and M. D. Lukin, Probing many-body dynamics on a 51-atom quantum simulator, Nature **551**, 579 (2017).

[22] H. Levine, A. Keesling, G. Semeghini, A. Omran, T. T. Wang, S. Ebadi, H. Bernien, M. Greiner, V. Vuletić, H. Pichler, and M. D. Lukin, Parallel Implementation of High-Fidelity Multiqubit Gates with Neutral Atoms, Phys. Rev. Lett. **123**, 170503 (2019).

[23] M. Cetina, L. N. Egan, C. A. Noel, M. L. Goldman, A. R. Risinger, D. Zhu, D. Biswas, and C. Monroe, Quantum gates on individually-addressed atomic qubits subject to noisy transverse motion (2020), ArXiv:2007.06768.

[24] I. Pogorelov, T. Feldker, C. D. Marciniak, L. Postler, G. Jacob, O. Krieglsteiner, V. Podlesnic, M. Meth, V. Negnevitsky, M. Stadler, B. Höfer, C. Wächter, K. Lakhmanskiy, R. Blatt, P. Schindler, and T. Monz, Compact ion-trap quantum computing demonstrator, PRX Quantum **2**, 020343 (2021).

[25] J. M. Pino, J. M. Dreiling, C. Figgatt, J. P. Gaebler, S. A. Moses, M. S. Allman, C. H. Baldwin, M. Foss-Feig, D. Hayes, K. Mayer, C. Ryan-Anderson, and B. Neyenhuis, Demonstration of the trapped-ion quantum CCD computer architecture, Nature **592**, 209 (2021).

[26] V. Kaushal, B. Lekitsch, A. Stahl, J. Hilder, D. Pijn, C. Schmiegelow, A. Bermudez, M. Müller, F. Schmidt-Kaler, and U. Poschinger, Shuttling-based trapped-ion quantum information processing, AVS Quantum Sci. **2**, 014101 (2020).

[27] C. Monroe and J. Kim, Scaling the ion trap quantum processor, Science **339**, 1164 (2013).

[28] T. E. Northup and R. Blatt, Quantum information transfer using photons, Nat. Photonics **8**, 356 (2014).

[29] D. Hucul, I. V. Inlek, G. Vittorini, C. Crocker, S. Debnath, S. M. Clark, and C. Monroe, Modular entanglement of atomic qubits using photons and phonons, Nat. Phys. **11**, 37 (2015).

[30] K. R. Brown, J. Kim, and C. Monroe, Co-designing a scalable quantum computer with trapped atomic ions, npj Quantum Inf. **2**, 16034 (2016).

[31] I. V. Inlek, C. Crocker, M. Lichtman, K. Sosnova, and C. Monroe, Multispecies Trapped-Ion Node for Quantum Networking, Phys. Rev. Lett. **118**, 250502 (2017).

[32] L. J. Stephenson, D. P. Nadlinger, B. C. Nichol, S. An, P. Drmota, T. G. Ballance, K. Thirumalai, J. F. Goodwin, D. M. Lucas, and C. J. Ballance, High-Rate, High-Fidelity Entanglement of Qubits across an Elementary Quantum Network, Phys. Rev. Lett. **124**, 110501 (2020).

[33] H. Takahashi, E. Kassa, C. Christoforou, and M. Keller, Cavity-induced anticorrelated photon-emission rates of a single ion, Phys. Rev. A **96**, 023824 (2017).

[34] H. Takahashi, E. Kassa, C. Christoforou, and M. Keller, Strong Coupling of a Single ion to an Optical Cavity, Phys. Rev. Lett. **124**, 013602 (2020).

[35] J. Schupp, V. Krcmarsky, V. Krutyanskiy, M. Meraner, T. Northup, and B. Lanyon, Interface between trapped-ion qubits and traveling photons with close-to-optimal efficiency, PRX Quantum **2**, 020331 (2021).

[36] N. Friis, O. Marty, C. Maier, C. Hempel, M. Holzäpfel, P. Jurcevic, M. B. Plenio, M. Huber, C. Roos, R. Blatt, and B. Lanyon, Observation of Entangled States of a Fully Controlled 20-Qubit System, Phys. Rev. X **8**, 021012 (2018).

[37] T. Pellizzari, S. A. Gardiner, J. I. Cirac, and P. Zoller, Decoherence, Continuous Observation, and Quantum Computing: A Cavity qed Model, Phys. Rev. Lett. **75**, 3788 (1995).

[38] A. S. Sørensen and K. Mølmer, Measurement Induced Entanglement and Quantum Computation with Atoms in Optical Cavities, Phys. Rev. Lett. **91**, 097905 (2003).

[39] J. Borregaard, P. Kómár, E. M. Kessler, A. S. Sørensen, and M. D. Lukin, Heralded Quantum Gates with Integrated Error Detection in Optical Cavities, Phys. Rev. Lett. **114**, 110502 (2015).

[40] L.-M. Duan, B. Wang, and H. J. Kimble, Robust quantum gates on neutral atoms with cavity-assisted photon scattering, Phys. Rev. A **72**, 032333 (2005).

[41] Y. Sun and P.-X. Chen, Analysis of atom-photon quantum interface with intracavity rydberg-blocked atomic ensemble via two-photon transition, Optica **5**, 1492 (2018).

[42] A. C. J. Wade, M. Mattioli, and K. Mølmer, Single-atom single-photon coupling facilitated by atomic-ensemble dark-state mechanisms, Phys. Rev. A **94**, 053830 (2016).

[43] L. Jiang, J. M. Taylor, A. S. Sørensen, and M. D. Lukin, Distributed quantum computation based on small quantum registers, Phys. Rev. A **76**, 062323 (2007).

[44] L. H. Pedersen and K. Mølmer, Few qubit atom-light interfaces with collective encoding, Phys. Rev. A **79**, 012320 (2009).

[45] D. Gottesman and I. L. Chuang, Demonstrating the viability of universal quantum computation using teleportation and single-qubit operations, Nature **402**, 390 (1999).

[46] K. S. Chou, J. Z. Blumoff, C. S. Wang, P. C. Reinhold, C. J. Axline, Y. Y. Gao, L. Frunzio, M. H. Devoret, L. Jiang, and R. J. Schoelkopf, Deterministic teleportation of a quantum gate between two logical qubits, Nature **561**, 368 (2018).

[47] B. W. Shore, Picturing stimulated raman adiabatic passage: A stirap tutorial, Adv. Opt. Photon. **9**, 563 (2017).

[48] C. D. Bruzewicz, J. Chiaverini, R. McConnell, and J. M. Sage, Trapped-ion quantum computing: Progress and challenges, Appl. Phys. Rev. **6**, 021314 (2019).

[49] See Supplemental Material http://link.aps.org/supplemental/10.1103/PRXQuantum.3.010344 for additional details regarding estimates of the ion implementation entanglement distribution speed and fidelity, and a discussion of the dependence of average nonlocal gate speed and storage error on connectivity and parallelizability.

[50] C. Crocker, M. Lichtman, K. Sosnova, A. Carter, S. Scarano, and C. Monroe, High purity single photons entangled with an atomic qubit, Opt. Express **27**, 28143 (2019).

[51] N. Kurz, M. R. Dietrich, G. Shu, R. Bowler, J. Salacka, V. Mirgon, and B. B. Blinov, Measurement of the branching ratio in the decay of barium with a single trapped ion, Phys. Rev. A **77,** 060501 (2008).

[52] R. Noek, G. Vrijsen, D. Gaultney, E. Mount, T. Kim, P. Maunz, and J. Kim, High speed, high fidelity detection of an atomic hyperfine qubit, Opt. Lett. **38,** 4735 (2013).

[53] S. Olmschenk, D. N. Matsukevich, P. Maunz, D. Hayes, L.-M. Duan, and C. Monroe, Quantum teleportation between distant matter qubits, Science **323,** 486 (2009).

[54] R. Nigmatullin, C. J. Ballance, N. de Beaudrap, and S. C. Benjamin, Minimally complex ion traps as modules for quantum communication and computing, New J. Phys. **18,** 103028 (2016).

[55] V. Aksyuk, *et al.*, 238 × 238 micromechanical optical cross connect, IEEE Photonics Technol. Lett. **15,** 587 (2003).

[56] A. Olkhovets, P. Phanaphat, C. Nuzman, D. Shin, C. Lichtenwalner, M. Kozhevnikov, and J. Kim, Performance of an optical switch based on 3-d mems crossconnect, IEEE Photonics Technol. Lett. **16,** 780 (2004).

[57] D. Kielpinski, C. Monroe, and D. J. Wineland, Architecture for a large-scale ion-trap quantum computer, Nature **417,** 709 (2002).

[58] H. Kaufmann, T. Ruster, C. T. Schmiegelow, M. A. Luda, V. Kaushal, J. Schulz, D. von Lindenfels, F. Schmidt-Kaler, and U. G. Poschinger, Fast ion swapping for quantum-information processing, Phys. Rev. A **95,** 052319 (2017).

[59] D. Gangloff, M. Shi, T. Wu, A. Bylinskii, B. Braverman, M. Gutierrez, R. Nichols, J. Li, K. Aichholz, M. Cetina, L. Karpa, B. Jelenković, I. Chuang, and V. Vuletić, Preventing and reversing vacuum-induced optical losses in high-finesse tantalum (v) oxide mirror coatings, Opt. Express **23,** 18014 (2015).

[60] M. Cetina, A. Bylinskii, L. Karpa, D. Gangloff, K. M. Beck, Y. Ge, M. Scholz, A. T. Grier, I. Chuang, and V. Vuletić, One-dimensional array of ion chains coupled to an optical cavity, New J. Phys. **15,** 053001 (2013).

[61] B. Casabone, A. Stute, K. Friebe, B. Brandstätter, K. Schüppert, R. Blatt, and T. E. Northup, Heralded Entanglement of two Ions in an Optical Cavity, Phys. Rev. Lett. **111,** 100505 (2013).

[62] M. Saffman, Quantum computing with atomic qubits and rydberg interactions: Progress and challenges, J. Phys. B: At., Mol. Opt. Phys. **49,** 202001 (2016).

[63] A. Georgakopoulos, *Modeling and Creating Cavity Rydberg Polaritons for Achieving Strongly Correlated Photonic Materials*, Ph.D. thesis, school The University of Chicago (2018).

[64] J. M. Auger, S. Bergamini, and D. E. Browne, Blueprint for fault-tolerant quantum computation with rydberg atoms, Phys. Rev. A **96,** 052320 (2017).

[65] R. Gehr, J. Volz, G. Dubois, T. Steinmetz, Y. Colombe, B. L. Lev, R. Long, J. Estève, and J. Reichel, Cavity-Based Single Atom Preparation and High-Fidelity Hyperfine State Readout, Phys. Rev. Lett. **104,** 203602 (2010).

[66] J. Volz, R. Gehr, G. Dubois, J. Estève, and J. Reichel, Measurement of the internal state of a single atom without energy exchange, Nature **475,** 210 (2011).

[67] A. D. Boozer, A. Boca, R. Miller, T. E. Northup, and H. J. Kimble, Cooling to the Ground State of Axial Motion for one Atom Strongly Coupled to an Optical Cavity, Phys. Rev. Lett. **97,** 083602 (2006).

[68] H. Mabuchi, Q. A. Turchette, M. S. Chapman, and H. J. Kimble, Real-time detection of individual atoms falling through a high-finesse optical cavity, Opt. Lett. **21,** 1393 (1996).

[69] M. Endres, H. Bernien, A. Keesling, H. Levine, E. R. Anschuetz, A. Krajenbrink, C. Senko, V. Vuletic, M. Greiner, and M. D. Lukin, Atom-by-atom assembly of defect-free one-dimensional cold atom arrays, Science **354,** 1024 (2016).

[70] Y. Wang, S. Shevate, T. M. Wintermantel, M. Morgado, G. Lochead, and S. Whitlock, Preparation of hundreds of microscopic atomic ensembles in optical tweezer arrays, npj Quantum Inf. **6,** 54 (2020).

[71] C. Monroe, R. Raussendorf, A. Ruthven, K. R. Brown, P. Maunz, L.-M. Duan, and J. Kim, Large-scale modular quantum-computer architecture with atomic memory and photonic interconnects, Phys. Rev. A **89,** 022317 (2014).

[72] D. Bluvstein, H. Levine, G. Semeghini, T. T. Wang, S. Ebadi, M. Kalinowski, A. Keesling, N. Maskara, H. Pichler, M. Greiner, V. Vuletic, and M. D. Lukin, A quantum processor based on coherent transport of entangled atom arrays, arXiv:2112.03923 [quant-ph] (2021).